Electronic Supplementary Material (ESI) for Journal of Materials Chemistry A.


Supplementary Information

# Formation of N-doped molybdenum carbide confined into hierarchical and hollow carbon nitride microspheres with enhanced sodium storage properties

Jiyicheng Qiu[a], Zhanxu Yang[a*], Qiang Li[a], Yue Li[b], Xian Wu[a], Chengyuan Qi[a], Qingdong Qiao[a]

[a] College of Chemistry, Chemical Engineering and Environment Engineering, Liaoning Shihua University, Fushun, Liaoning 113001, P. R. China.

[b] School of Foreign Languages, Liaoning Shihua University, Fushun, Liaoning 113001, P. R. China

*Corresponding author: zhanxuy@126.com(Z. Yang).

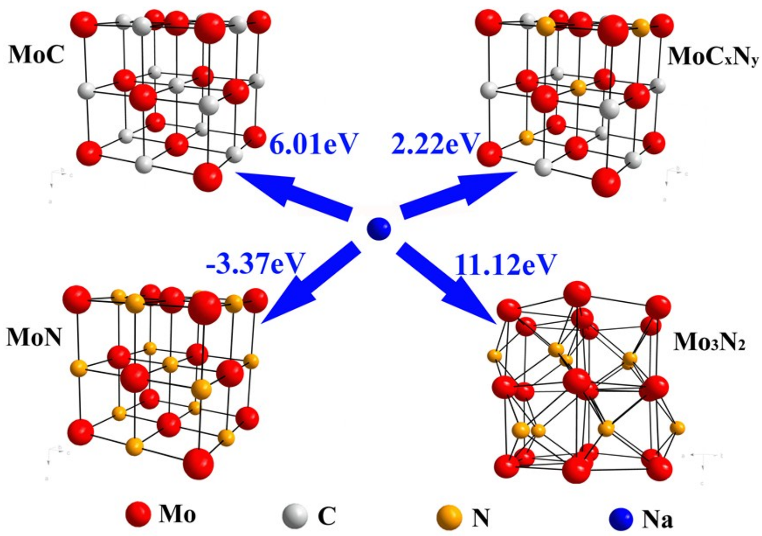


**Fig. S1** The first-principles calculation results of binding energy difference upon the sodium ion absorption into various molybdenum carbide or nitride.

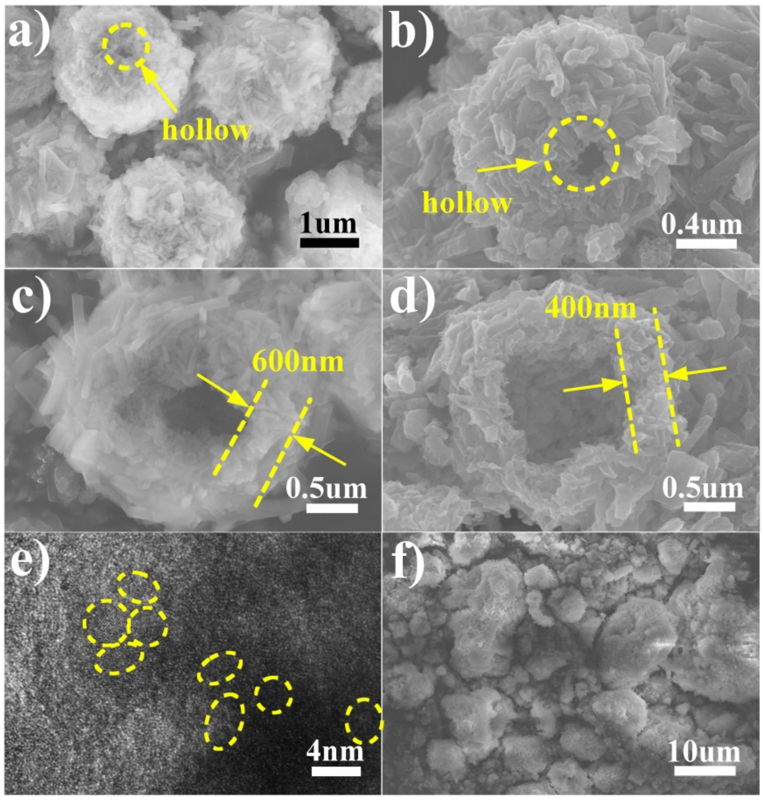


**Fig. S2** (a) SEM image of melamine-based supramolecular precursor show the hollow structure. (b) SEM image of PM-500 reveal that the annealed sample also maintain the hollow structure. (c) SEM image of broken melamine-based supramolecular microsphere. (d) SEM image of broken PM-500 microsphere. (e) TEM image of PM-500 sample show the uniform dispersion of $MoC_xN_y$ nanoparticles. (f) SEM image of the melamine-based supramolecular samples without addition of L-glutamic acid

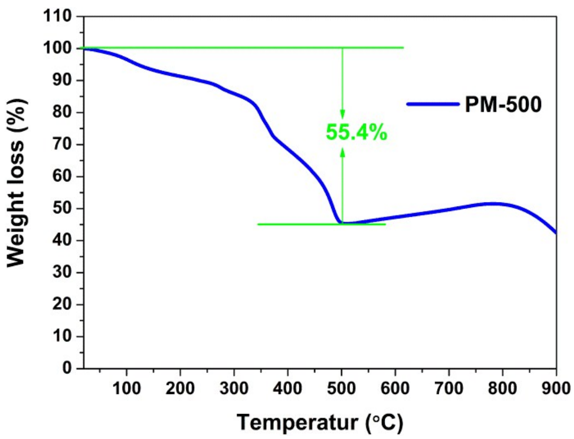


**Fig. S3** TG analysis for the calcination of melamine-based supramolecular precursor up to 900 °C in $N_2$ gas.

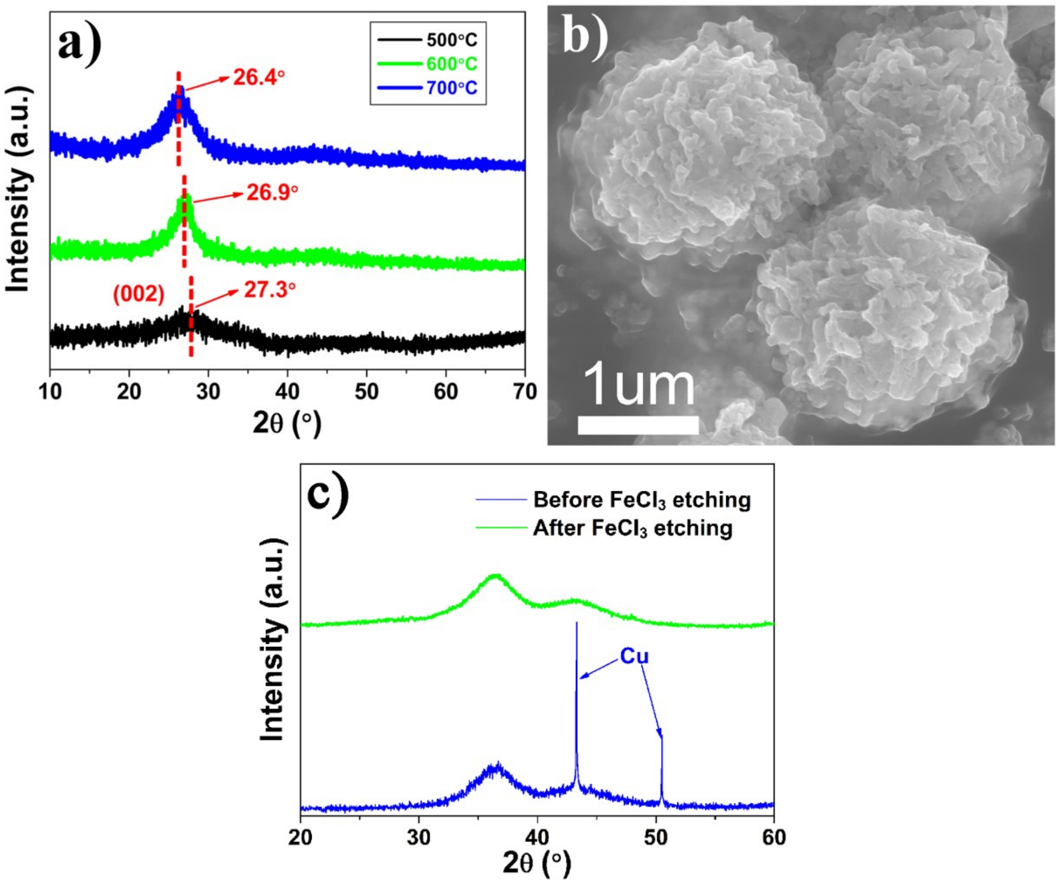


**Fig. S4** (a) XRD pattern and (b) SEM image of the as-obtained carbon nitride matrix. (c) XRD pattern of the calcined composites before and after $FeCl_3$ etching treatment.

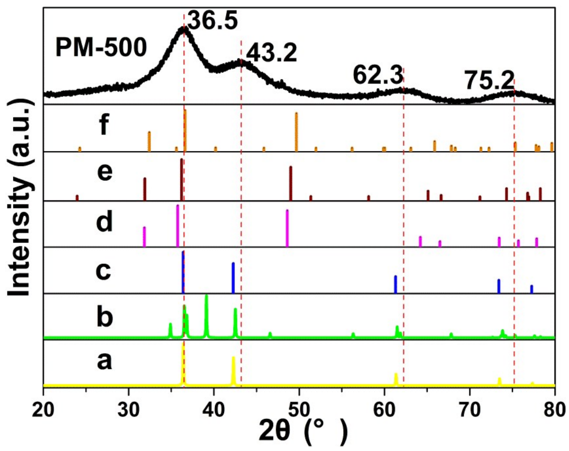


**Fig. S5** XRD pattern comparison for PM-500 with (a) $MoC_{1-x}$ (JCPDS 01-89-2868), (b) $MoC_{1-x}$ (JCPDS 01-089-4305), (c) MoC (JCPDS 65-0280), (d) MoC (JCPDS 65-6664), (e) MoN (JCPDS 25-1367) and (f) MoN (JCPDS 89-2904).

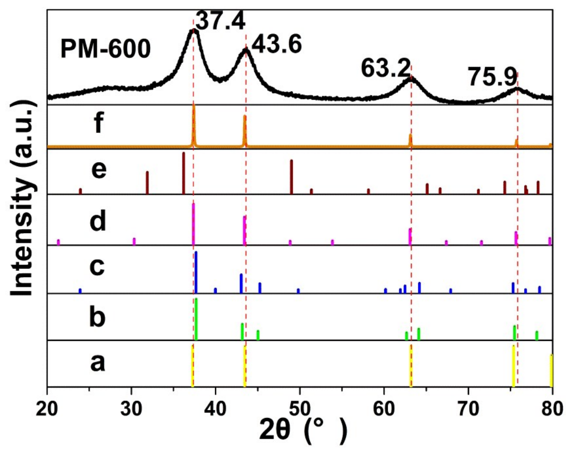


**Fig. S6** XRD pattern comparison for PM-600 with (a) $Mo_2N$ (JCPDS 03-0907), (b) $Mo_2N$ (JCPDS 25-1368), (c) $No_2N$ (JCPDS 65-6236), (d) $Mo_3N_2$ (JCPDS 65-4278), (e) MoN (JCPDS 25-1367) and (f) $Mo_2N$ (JCPDS 25-1366)

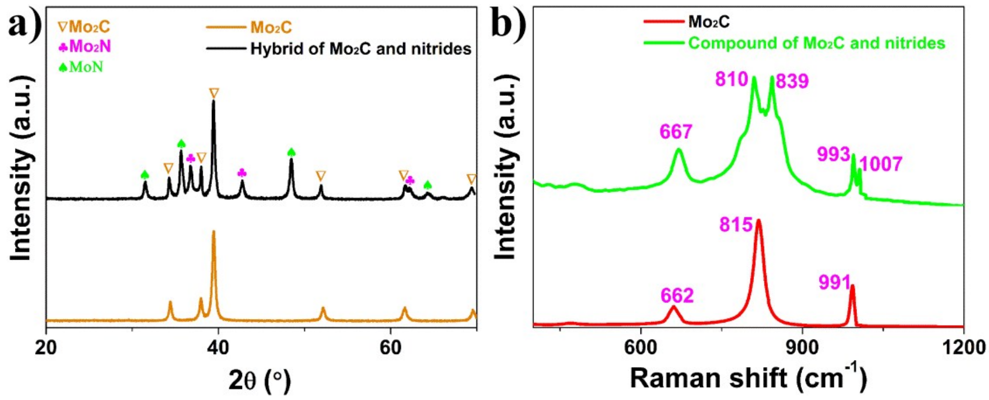


**Fig. S7** (a) The XRD pattern of pure $Mo_2C$ and the mixture compound of pure $Mo_2C$, MoN and $Mo_2N$. (b) the Raman spectra of pure $Mo_2C$ and the mixture compound of pure $Mo_2C$, MoN and $Mo_2N$.

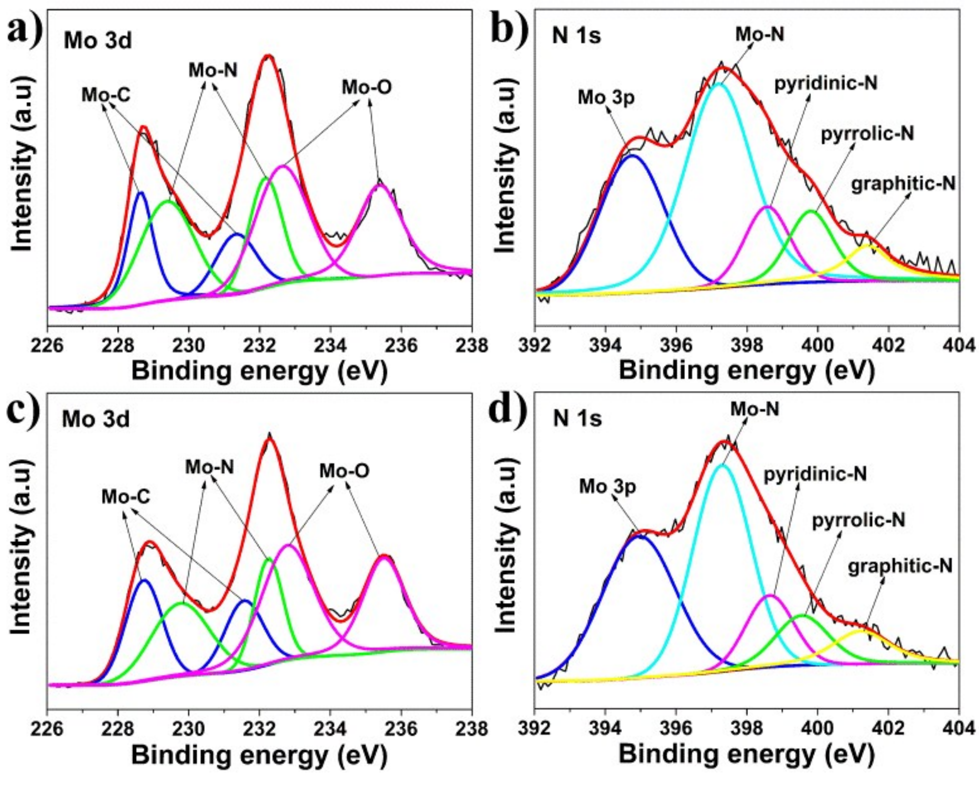


**Fig. S8** XPS spectra of PM-500 for (a) Mo3*d* and (b) N1*s*. XPS spectra of PM-700 for (c) Mo3*d* and (d) N1*s*.

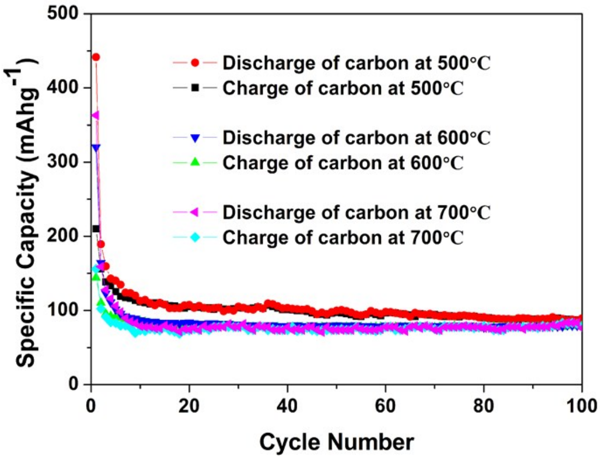


**Fig. S9** Cyclability tests on the as-obtained carbonaceous materials calcined at 500, 600 and 700 $^oC$ at a current density of 0.16 A $g^{-1}$ for 100 cycles.

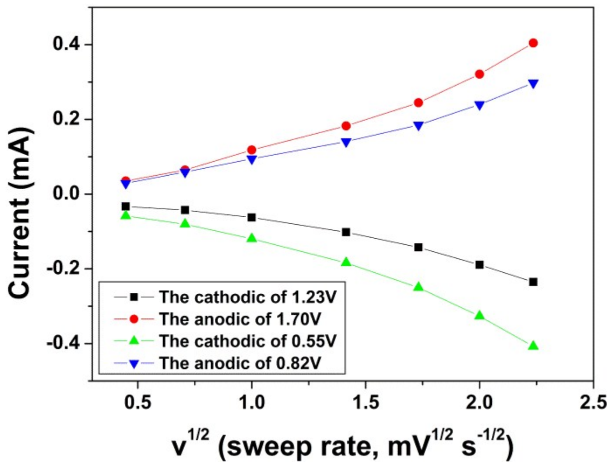


**Fig. S10** The Relationship between the peak current and the square root of sweep rates

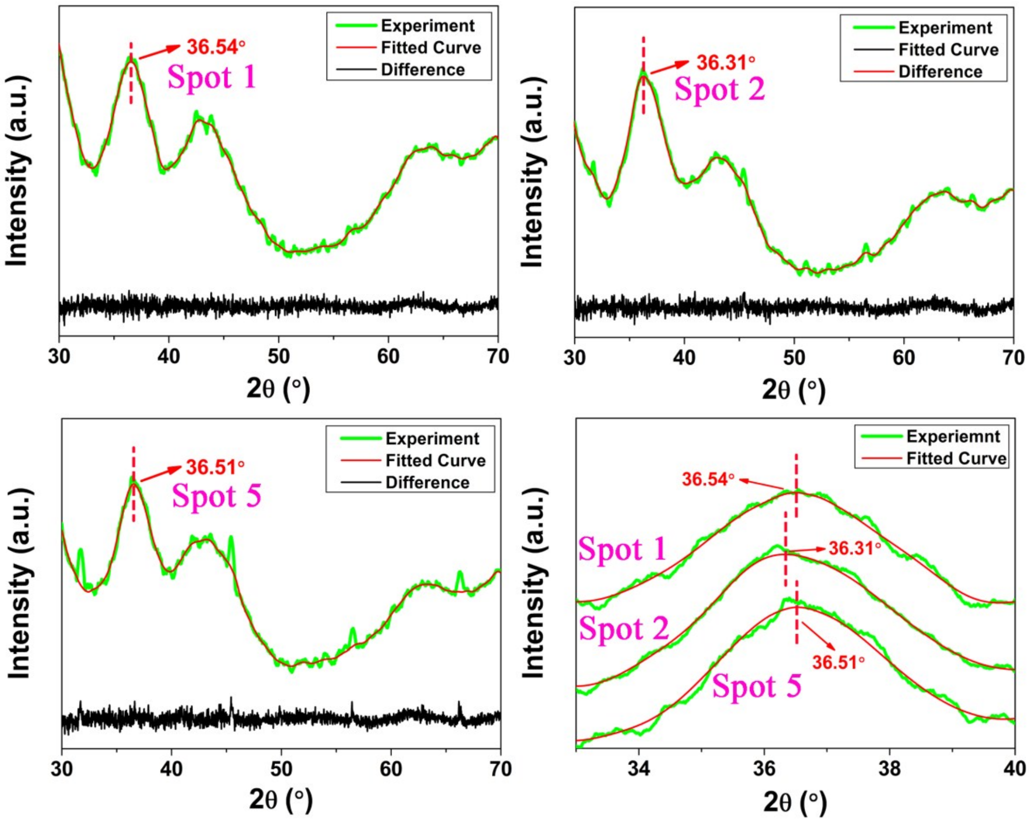


**Fig. S11** The fitted XRD pattern of the PM-500 electrode (a) without cycling (spot 1), (b) at the discharge potential 0.9 V (spot 2) and (b) charge potential 3 V (spot 5) by TOPAS software. (d) The 2θ region 33~40 ° magnification for the fitted XRD pattern of the electrode at the above three step. (spot 3: discharge to 0.01 V; spot 4: charge to 1.4 V)

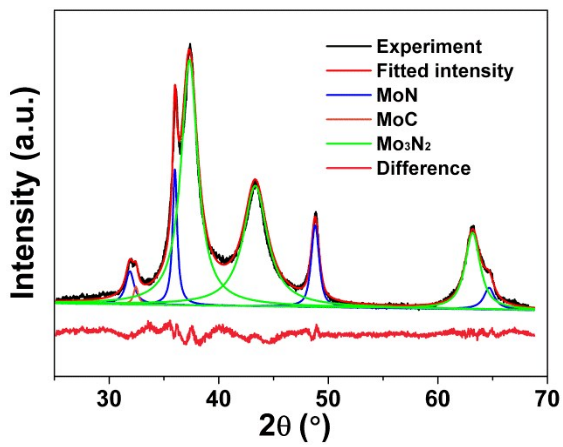


**Fig. S12** The TOPAS analysis on XRD pattern of the PM-700 composites.

**Table S1** Characteristics of the deconvoluted Mo3*d* spectra for various composites

| Sample | Peak Position (eV) | | | Species Percentage (%) | | |
|---|---|---|---|---|---|---|
| | Mo-C | Mo-N | Mo-O | Mo-C | Mo-N | Mo-O |
| PM-500 | 228.4 ; 230.9 | 229.1 ; 231.9 | 232.6 ; 235.5 | 22.62 | 33.72 | 41.66 |
| PM-600 | 228.6 ; 231.3 | 229.4 ; 232.2 | 232.6 ; 235.4 | 18.48 | 37.61 | 43.91 |
| PM-700 | 228.8 ; 231.6 | 229.8 ; 232.4 | 232.7 ; 235.5 | 11.27 | 45.94 | 42.79 |

**Table S2** Characteristics of the deconvoluted N1*s* spectra for various composites

| Species | Peak Position (eV) | | | Species Percentage (%) | | |
|---|---|---|---|---|---|---|
| | PM-500 | PM-600 | PM-700 | PM-500 | PM-600 | PM-700 |
| Mo-N | 397.1 | 397.2 | 397.3 | 55.87 | 57.7 | 58.13 |
| pyridinic-N | 398.2 | 398.6 | 398.6 | 17.03 | 18.62 | 16.51 |
| pyrrolic-N | 399.5 | 399.8 | 399.6 | 15.66 | 14.22 | 14.01 |
| graphitic-N | 400.9 | 401.3 | 401.2 | 11.44 | 9.46 | 11.35 |

**Table S3** Refined parameters of molybdenum carbonitride at various potential steps and the cell parameters of Pristine α-$MoC_{1-x}$ (JCPDS 01-89-2868)

| Samples | Refined lattice parameters |
|---|---|
| $MoC_xN_y$ with no cycling (Spot 1) | *a*=*b*=*c*=4.137±0.003 Å |
| $MoC_xN_y$ discharged to 0.9V (Spot 2) | *a*=*b*=*c*=4.172±0.004 Å |
| $MoC_xN_y$ charged to 3V (Spot 5) | *a*=*b*=*c*=4.151±0.002 Å |
| Pristine α-$MoC_{1-x}$ | *a*=*b*=*c*=4.270 Å |

**Table S4** Comparison for electrochemical properties of various anode materials for sodium ion batteries

| Materials | Current rate (mA $g^{-1}$) | Specific capacity (mAh $g^{-1}$) | Ref |
|---|---|---|---|
| $MgFe_2O_4$/reduced graphene oxide | 100 | 306 | 1 |
| | 500 | 197.6 | |
| $TiO_2$/C | 100 | 221 | 2 |
| | 500 | 173 | |
| Cu-doped $Li_4Ti_5O_{12}$/carbon nanofiber | 100 | 123 | 3 |
| | 400 | 79 | |
| $SnO_2$/carbon fiber | 100 | 359 | 4 |
| | 400 | 251 | |
| $FePO_4$@MCNT nanowire | 0.3 C | 133.2 | 5 |
| | 0.5C | 122.2 | |
| $Sn_3N_4$ nanocrystal | 200 | 164 | 6 |
| | 400 | 127 | |
| carbon-coated $TiO_2$ | 100 | 183 | 7 |
| | 400 | 149 | |
| MoS2 nanosheets | 160 | 305 | 8 |
| | 320 | 251 | |
| $MoC_xN_y$/carbon nitride hollow microsphere | 160 | 410 | Our work |
| | 500 | 310 | |

## References


1 X Zhang, T Chen, D Yan, W Qin, B Hu, Z Sun and L Pan, $MgFe_2O_4$/reduced graphene oxide composites as high-performance anode materials for sodium ion batteries, Electrochim. Acta., 2015, **180**, 616-621.

2 C. Ding, T. Nohira and R. Hagiwara, A high-capacity $TiO_2$/C negative electrode for sodium secondary batteries with an ionic liquid electrolyte, J. Mater. Chem. A, 2015, **3**, 20767-20771.

3 Y. Ge, H. Jiang, K. Fu, C. Zhang, J. Zhu, C. Chen, Y. Lu, Y. Qiu and X. Zhang, Copper-doped $Li_4Ti_5O_{12}$/carbon nanofiber composites as anode for high-performance sodium-ion batteries, J. Power Sources, 2014, **272**, 860-865.

4 M. Dirican, Y. Lu, Y. Ge, O. Yildiz and X. Zhang, Carbon-Confined $SnO_2$-Electrodeposited Porous Carbon Nanofiber Composite as High-Capacity Sodium-Ion Battery Anode Material, ACS Appl. Mater. Interfaces, 2015, **7**, 18387-18396.

5 S. Xu, S. Zhang, J. Zhang, T. Tan and Y. Liu, A maize-like $FePO_4$@MCNT nanowire composite for sodium-ion batteries via a microemulsion technique, J. Mater. Chem. A, 2014, **2**, 7221-7228.

6 X. Li, A. L. Hector, J. R. Owen and S. I. U. Shah, Evaluation of nanocrystalline $Sn_3N_4$ derived from ammonolysis of $Sn(NEt_2)_4$ as a negative electrode material for Li-ion and Na-ion batteries, J. Mater. Chem. A, 2016, **4**, 5081-5087.

7 Y. Ge, H. Jiang, J. Zhu, Y. Lu, C. Chen, Y. Hu, Y. Qiu and X. Zhang, High cyclability of carbon-coated $TiO_2$ nanoparticles as anode for sodium-ion batteries, Electrochim. Acta., 2015, **157**, 142-148.

8 D. Su, S. Dou and G. Wang, Ultrathin $MoS_2$ Nanosheets as Anode Materials for Sodium-Ion Batteries with Superior Performance, Adv. Energy Mater., 2015, **5**, 1401205.